Marine Chemistry 207 (2018) 26–32

Contents lists available at ScienceDirect

Marine Chemistry

journal homepage: www.elsevier.com/locate/marchem

Henry's Law constant for CO_2 in aqueous sodium chloride solutions at 1 atm and sub-zero (Celsius) temperatures

Neal Bailey[a], Tim N. Papakyriakou[a], Carl Bartels[b], Feiyue Wang[a,*]

[a] Centre for Earth Observation Science, and Department of Environment and Geography, University of Manitoba, Winnipeg, MB R3T 2N2, Canada
[b] Department of Chemistry, University of Manitoba, Winnipeg, MB R3T 2N2, Canada

ARTICLE INFO

Keywords:
Carbon dioxide
Henry's Law constant
Solubility
Seawater

ABSTRACT

The solubility of CO_2 in seawater is known to increase at colder temperatures, but few studies have examined the CO_2 solubility in seawater and in sea-ice brines at sub-zero (Celsius) temperatures. The thermodynamic Henry's Law constant (K_H) for CO_2 in concentrated NaCl solutions was determined for the first time at sub-zero temperatures and salinities resembling those of the cryospheric seawater and sea-ice brine environments in polar and sub-polar oceans. The temperature (T, in Kelvin) dependence of the K_H within the temperature and salinity ranges of this study ($263 \leq T \leq 272$ K and $35 \leq S \leq 152$) is described by the following best-fit equation: $\ln K_H = -2.484 + 2.775 \times 10^{-2}(274 - T) - 9.854 \times 10^{-2}/(274 - T) - 1.009 \times 10^{-1} \ln(274–T)$. The results show that the general practice, in geochemical and coupled climate-carbon cycling models, of extrapolating K_H values from above-zero to sub-zero temperatures underestimates the solubility of CO_2 by up to 19%.

1. Introduction

The oceanic reservoir of CO_2 is 50 times larger than its atmospheric reservoir, and ultimately determines the atmospheric CO_2 concentrations on any time scale longer than a few hundred years (Sarmiento and Gruber, 2006). Recent estimates suggest that the global ocean has absorbed on average 2.6×10^{15} gC yr^{-1}, or 25% of the total anthropogenic CO_2 emissions over the last decade (2006–2015) (Le Quéré et al., 2016), amounting to a total of $\sim 155 \times 10^{15}$ gC of anthropogenic CO_2 as of 2010 (Khatiwala et al., 2013). The ocean absorbs a large amount of CO_2 because of the relatively high solubility of CO_2 in seawater, with the dissolved CO_2 participating in chemical and biological processes while being circulated around the global ocean; this results in generally negative partial pressure (pCO_2) gradients at the air-sea interface which drive CO_2 uptake by the ocean. The solubility of CO_2 in seawater, often measured as the Henry's Law constant (K_H), is thus one of the most important properties in understanding regional and global carbon cycles and their coupling with climate. It has been well established that the solubility of CO_2 in seawater increases at colder temperatures (Weiss, 1974), making the high-latitude oceans especially efficient in CO_2 uptake (Takahashi et al., 2009, 2014). Nevertheless, whereas K_H for CO_2 in seawater has been studied extensively (see reviews in Carroll et al. (1991); Plummer and Busenberg (1982); Weiss (1974)), only a few experimental studies were carried out at temperatures colder than 10 °C. Of the 84 data points from the literature reanalyzed by Plummer and Busenberg (1982), only 11 were obtained at or below 10 °C. Most notably, only one study extended the solubility of CO_2 into the sub-zero (Celsius) temperatures, with a single data point obtained at −5 °C in artificial seawater (Stewart and Munjal, 1970). This data gap represents a major challenge in our understanding of the carbon cycle in polar oceans where the surface seawater temperature can be seasonally below 0 °C.

CO_2 exchange between the atmosphere and polar oceans is further complicated by sea-ice freeze-thaw cycles that are both inherently dynamic and profoundly impacted by climate change. Arctic sea ice has been undergoing rapid changes over the past four decades, becoming warmer, younger, and thinner (Meier, 2017) and with increased permeability for gases such as CO_2 (Miller et al., 2011). The recent discovery of ikaite ($CaCO_3 \cdot 6H_2O$) in sea ice (Dieckmann et al., 2008, 2010; Rysgaard et al., 2011, 2013, 2014) reveals that the carbonate chemistry of the sea ice-brine system, where temperature can reach as low as −20 °C, may play an important role in the air-sea exchange of CO_2 in polar oceans (Rysgaard et al., 2011, 2013). Brines formed during freeze-up processes can be enriched in CO_2 due to dissolution of ikaite, and may sequester this CO_2 in deeper waters below the mixed layer (Anderson et al., 2004; Rysgaard et al., 2007). Estimates of uptake of atmospheric CO_2 associated with these processes range from 1–4% (Grimm et al., 2016; Moreau et al., 2016) to 9–20% (Rysgaard et al.,

* Corresponding author.
E-mail address: feiyue.wang@umanitoba.ca (F. Wang).

https://doi.org/10.1016/j.marchem.2018.10.003
Received 27 February 2018; Received in revised form 8 October 2018; Accepted 15 October 2018
Available online 17 October 2018
0304-4203/ © 2018 The Authors. Published by Elsevier B.V. This is an open access article under the CC BY-NC-ND license (http://creativecommons.org/licenses/BY-NC-ND/4.0/).

2011) of current net oceanic uptake in Arctic regions, and 2–12% (Grimm et al., 2016; Moreau et al., 2016) to 42–116% (Rysgaard et al., 2011) in Antarctic regions. This wide range of uptake estimates suggests significant uncertainty in the behavior and characteristics of these CO_2-rich brines.

In the absence of experimental data, the solubility of CO_2 in seawater at sub-zero temperatures has so far been simply extrapolated from K_H values that were determined at above 0 °C. For instance, most coupled climate-carbon cycle models (Orr et al., 2017) calculate the CO_2 solubility in seawater from a temperature (t in °C, or T in Kelvin) and salinity (S) function derived by Weiss (1974), which was based on a reanalysis of experimental data of Murray and Riley (1971) obtained at $1 \le t \le 35$ °C and $0 \le S \le 37.4$. Similarly, FREZCHEM, a cold-temperature equilibrium chemical thermodynamic model (Marion and Kargel, 2008), estimates the CO_2 solubility at sub-zero temperatures from a function derived by Plummer and Busenberg (1982), itself based on a reanalysis of literature data obtained at $0 \le t \le 325$ °C. The reliability of extrapolating K_H values of CO_2 obtained at above-zero to sub-zero temperatures has never been verified experimentally, but a similar extrapolation has recently been shown to produce large discrepancies in the dissociation constants of carbonic acid in seawater-derived brine at sub-zero temperatures when compared with experimentally determined values (Papadimitriou et al., 2018).

Here, we report the determination of K_H for CO_2 in NaCl solutions at temperatures between −1 and − 10 °C. We chose to determine K_H for CO_2 in NaCl solutions instead of in seawater or seawater-derived brines to avoid the compositional change that accompanies the precipitation of minerals from seawater (e.g., ikaite, mirabilite) at sub-zero temperatures (Papadimitriou et al., 2018). The use of the simple electrolyte NaCl, which contains the most abundant cation and anion in natural seawater, also allows us to correct for activity coefficients to obtain matrix-independent thermodynamic (K_H) values instead of stoichiometric (K_H^*) values. Such thermodynamic K_H values can be applied to seawater and brines of varying ionic compositions to calculate the aqueous CO_2 concentration, provided that the ionic composition of the seawater or brine is known and the activity coefficients can be reliably estimated.

2. Principle

Assuming CO_2 reaches equilibrium between the gas and aqueous phases, K_H is defined as:

$$CO_2(g) = CO_2(aq) \quad (1)$$

$$K_H^* = \frac{m_{CO_2(aq)}}{pCO_2} \quad (2)$$

$$K_H = \frac{a_{CO_2(aq)}}{f_{CO_2(g)}} = \frac{\gamma_{CO_2(aq)}}{\gamma_{CO_2(g)}} \cdot \frac{m_{CO_2(aq)}}{pCO_2} = \frac{\gamma_{CO_2(aq)}}{\gamma_{CO_2(g)}} K_H^* \quad (3)$$

where a_i, f_i, m_i, p_i, γ_i denote activity, fugacity, molality, partial pressure and activity coefficient of species i, respectively. The stoichiometric (or conditional) Henry's Law constant, K_H^*, as defined in Eq. (2), is dependent not only on T and pressure (P), but also on the chemical composition of the solution. In contrast, the thermodynamic Henry's Law constant, K_H, as defined in Eq. (3), is based on activities and is thus only dependent on T and P. Unless otherwise specified, all the K_H and K_H^* values reported herein are reported at P = 1 atm and on the molal scale with pCO_2 in the unit of atm, i.e., mol (kg H_2O)$^{-1}$ atm^{-1}.

Whereas pCO_2 can be readily measured with a real-time CO_2 analyzer, the determination of $m_{CO_2}(aq)$ is not straightforward because CO_2(aq) undergoes dissociation in water:

$$CO_2(aq) + H_2O = H^+ + HCO_3^- \quad K_{a1} \quad (4)$$

$$HCO_3^- = H^+ + CO_3^{2-} \quad K_{a2} \quad (5)$$

Carbonic acid (H_2CO_3) is not shown in Eq. (4) as it only accounts for ~0.15% of the CO_2(aq) concentration (Millero, 2013). To calculate the concentration of CO_2(aq) from the measured total dissolved inorganic carbon (DIC):

$$m_{DIC} = m_{CO_2(aq)} + m_{HCO_3^-} + m_{CO_3^{2-}} \quad (6)$$

one needs to know the values of the carbonic acid dissociation constants K_{a1} and K_{a2} and the pH of the solution. Based on new experimental data, Papadimitriou et al. (2018) recently reported the temperature ($-6 \le t \le 25$ °C) and salinity ($33 \le S \le 100$) dependence functions of the stoichiometric K_{a1}^* and K_{a2}^* values, but cautioned that these functions cannot be extrapolated to T and S conditions outside of their experimental ranges. In determining the K_{a1}^* and K_{a2}^* values at sub-zero temperatures, Papadimitriou et al. (2018) also relied on extrapolated K_H values based on Weiss (1974). Uncertainties also exist with the accuracy of pH measurements in highly concentrated solutions (e.g., $S > 35$) at sub-zero temperatures (Hare et al., 2013; Papadimitriou et al., 2018).

To overcome these uncertainties, this study exploits a special relationship between DIC and total alkalinity (TA) to solve for $m_{CO_2}(aq)$. In the absence of other weak acids and bases, the TA in the NaCl-$NaHCO_3$ solutions used in this study can be defined as:

$$m_{TA} = m_{HCO_3^-} + 2m_{CO_3^{2-}} + m_{OH^-} - m_{H^+} \quad (7)$$

Combining Eqs (6) and (7) yields:

$$m_{CO_2(aq)} = m_{DIC} - m_{TA} + m_{CO_3^{2-}} + m_{OH^-} - m_{H^+} \quad (8)$$

The K_{a1} and K_{a2} of carbonic acid have been determined in NaCl solutions (to 6 mol kg^{-1}) and to 0 °C (He and Morse, 1993), but not at below-zero temperatures. Their values under our experimental temperature ($-10 \le t \le -1$ °C) and salinity ($35 \le S \le 152$) conditions are not known precisely. Nevertheless, estimates based on the recent equations of Papadimitriou et al. (2018) and the equations used in FREZCHEM (Marion and Kargel, 2008) both suggest that they are in the range of 6.0–7.0 and 9.5–11.0, respectively. Therefore, by fixing the pH of the solution within the range of 6.0–7.5, $m_{CO_2}(aq) >> 100\ m_{CO_3^{2-}}$, making $m_{CO_3^{2-}}$ in Eq. (8) negligible. Likewise, if ($m_{DIC} - m_{TA}$) is maintained at $> 10^{-4}$ mol kg^{-1}, m_{H^+} and m_{OH^-} in Eq. (8) can also be neglected. Under such conditions, Eq. (8) simplifies to:

$$m_{CO_2(aq)} \approx m_{DIC} - m_{TA} \quad (9)$$

K_H^* and K_H can thus be calculated as:

$$K_H^* \approx \frac{m_{DIC} - m_{TA}}{pCO_2} \quad (10)$$

$$K_H \approx \frac{\gamma_{CO_2(aq)}}{\gamma_{CO_2(g)}} \cdot \frac{m_{DIC} - m_{TA}}{pCO_2} \quad (11)$$

In this study, γ_i in concentrated electrolyte solutions at sub-zero temperatures are calculated by the FREZCHEM model (Version 13.3) (Marion and Kargel, 2008) using the Pitzer approach (Pitzer, 1995).

3. Experimental

3.1. Experimental set-up and analyses

The CO_2 solubility experiments were carried out inside a Honeywell-controlled cold room laboratory (temperature adjustable from 4 to −40 °C) at the University of Manitoba (Fig. 1). The room temperature was pre-set to the desired value before the experiment started. Further control of the temperature was achieved by placing the 1-L PTFE reaction vessel with multiple ports (Savillex) in an Anova A25 Refrigerated and Heating Circulator inside the cold room, set to the same desired temperature ± 0.01 °C of each run. The CO_2 solubility was determined in unfrozen solutions with three to five replicates at four temperatures (−1, −2, −5 and − 10 °C) and three NaCl concentrations (0.62, 2.09 and 3.07 mol (kg H_2O)$^{-1}$, or 34.9, 108.8, and

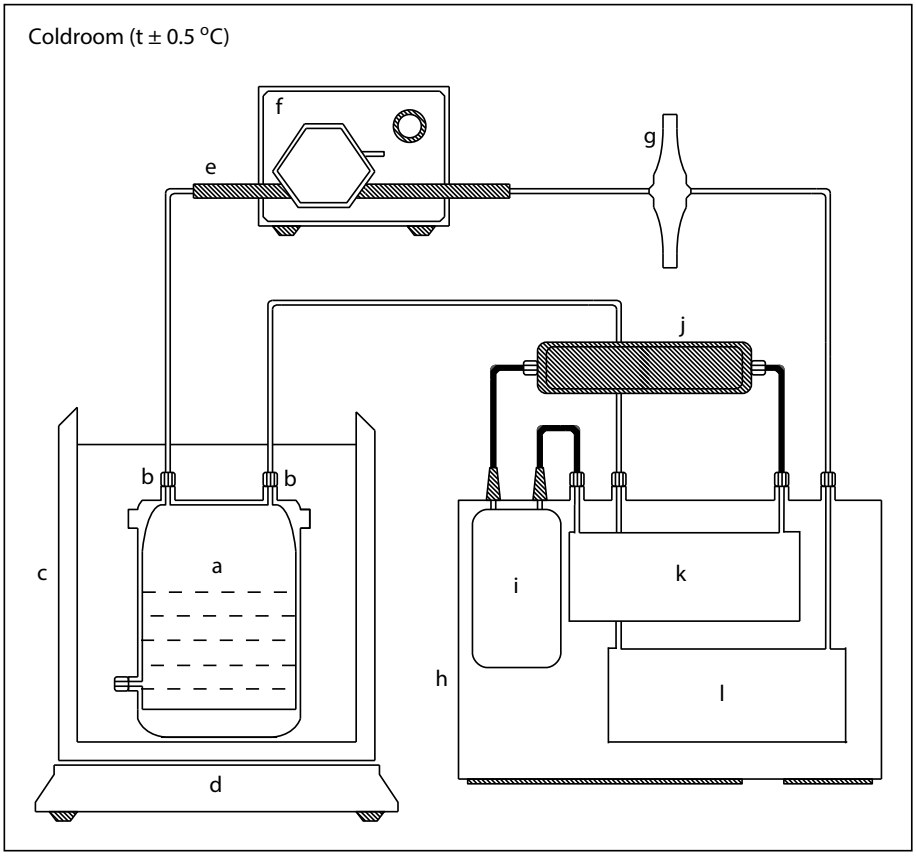

Fig. 1. Schematics showing the experimental set-up for determining the Henry's Law constant for CO_2 at sub-zero temperatures.

151.9 g (kg solution)$^{-1}$, respectively). The freezing points of the NaCl solutions were − 2.07, −7.32, and − 11.18 °C, respectively (Potter et al., 1978), and the experimental temperatures were at least 1 °C warmer than the corresponding freezing point to ensure the solution remained ice-free. These T–NaCl concentration combinations were chosen to represent the broad T-S range of the unfrozen, cold seawater and sea-ice brine.

For each run, 600 mL of a NaCl solution of a specific concentration, prepared by dissolving NaCl (Fisher Scientific) in Milli-Q water (Millipore), was added to the reaction vessel; the density of the solution was determined gravimetrically (the relative error was about 0.2%). About 50 mg of $NaHCO_3$ (ACS Reagent Grade, Sigma Aldrich) and ~ 1 mL of 0.1 M HCl (Fisher Scientific) were then added to the vessel to buffer the system and to adjust the pH. The exact amounts of $NaHCO_3$ and HCl required were estimated based on FREZCHEM to achieve the desired pH range (6.0–7.5). To allow for real-time measurements of the pCO_2 in the reactor headspace, the top sampling port of the reaction vessel was connected through a closed, gas-tight, PFA loop (see Fig. 1) and a peristaltic pump, set at a fixed rate of 1.5 L min^{-1}, to a solid-state, near infra-red CO_2 analyzer (LI-COR, Model LI-7000), also located inside the cold room set at the temperature of interest. The CO_2 analyzer was calibrated via a two-point span, using the CO_2 calibration standard gases at 906.855 μmol mol^{-1} and 2169.907 μmol mol^{-1} (NOAA ESRL/GMD); these concentrations were selected to encompass the expected range of the headspace pCO_2. The CO_2 measurements from the LI-COR-7000 were given as mixing ratios (mol mol^{-1}) and were converted to pCO_2 based on the atmospheric pressure (all the experiments were carried out at barometric pressures within 2% deviation from the standard atmospheric pressure of 1 atm) and water vapor pressure, which was simultaneously measured by the instrument. Calibrations were conducted at each temperature, and the accuracy of the CO_2 analyzer was assessed with the standard gases before and after experimental runs. The reference cell was maintained at zero CO_2 and zero water vapor content by pumping the cell gas through a closed loop containing an Ascarite II (NaOH-coated silica)/$Mn(ClO_4)_2$ scrubber.

The reaction vessel and temperature bath were mounted on a Labshake heavy load shaker (Gerhardt Bonn), set at 47 rpm, for a minimum of 16 h to ensure equilibrium between the aqueous and air phases, which was indicated by a constant pCO_2 in the headspace. Twenty mL samples for DIC analysis were then withdrawn from the bottom port of the reaction vessel through a gas-tight septum via a glass syringe. Samples for TA analysis were collected after the DIC sampling, through the other top port of the reaction vessel after it was removed from the cold room.

The DIC and TA analyses were performed at room temperature at the University of Manitoba. The DIC analyses were carried out using an Apollo SciTech DIC analyzer, following acidification by 10% (v/v) phosphoric acid (Fisher Scientific). N_2 gas (99.998% purity, Praxair) was used as the carrier and zero gas, and a daily calibration was performed with a seawater certified reference material (CRM; DIC = 2031.53 μmol (kg sw)$^{-1}$; Batch 144, Scripps Institute of Oceanography). The calibration was carried out using a four-point regression with the standard solution varying between 0.25 and 0.75 mL in a 0.75 mL total volume injection; calibration curves were considered valid when the measurement of the CRM was within 1% of the stated value. CRM measurements were typically reproducible to within

~0.1%.

The TA analyses were carried out by titrating the sample with 0.0500 M HCl (Trace Grade, Alfa Aesar; not matched to the experimental solution ionic strength) on a TIM 840 potentiometric titrator with a SAC850 Radiometer Analytical Sample Changer (Hach), following the modified open-cell method of Dickson et al. (2003). The mass of each sample (ranging from 12 to 20 g) and the salinity were measured and incorporated in the determination of TA. The TA sample temperatures were not held constant but were continually monitored by a combined temperature and pH probe throughout the titrations; corrections to the measured pH were automatically applied by the TIM 840 system. Daily calibration for the TA analyses was accomplished using pH standards (Ricca Chemical). The quality control checks were conducted by running a seawater CRM (TA = 2238.60 μmol (kg sw)$^{-1}$; Batch 144, Scripps Institute of Oceanography) every 10 samples, and the results were 99.0 ± 1.0% (n = 140 over the study period) of the reported CRM value.

The measured TA and DIC in units of μmol (kg sln) $^{-1}$ were converted to molality (μmol (kg H_2O) $^{-1}$) from the difference between the mass of the solute (NaCl) and the mass of the solution, both of which were measured gravimetrically.

3.2. Curve fitting

The temperature (in Kelvin) dependence expression for K_H was computed using the data obtained from this study, and in combination with the literature data. The computation was done using the regression wizard of the computer program SigmaPlot (Version 13, Systat Software Inc.) with an equation of the following form (Plummer and Busenberg, 1982):

$$\ln K_H = a_1 + a_2 T + a_3/T + a_4 \ln T + a_5/T^2 \quad (12)$$

where a_i are fitting parameters. To be consistent with Plummer and Busenberg (1982), the fitting was done with the inverse of the standard deviation of ln K_H as a weighting factor. That is, the computed values predict more closely the experimental values that are associated with smaller standard deviations.

4. Results

The experimental data from the determinations of the stoichiometric K_H^* and thermodynamic K_H for CO_2 are shown in Table 1. The average values and uncertainties of K_H at different temperatures are shown in Table 2, with K_H increasing from 8.87×10^{-2} at −1 °C to 1.43×10^{-1} at −10 °C.

In estimating the uncertainties, measured as the standard deviation s, errors from four sources were taken into consideration:

1) Methodological errors associated with simplifying Eq. (8) to Eq. (9). For Eq. (9) to be valid, the pH of the experimental solutions needs to be set such that $m_{CO_3^{2-}}$, m_{H^+} and m_{OH^-} are all negligible when compared to $m_{DIC} - m_{TA}$. As shown in Table 1, the approximate pH of the experimental solutions, as estimated using FREZCHEM, were in a narrow range of 6.6–7.2. Even if the actual pH of the solution were to deviate over 0.5 units, our calculations using the carbonic acid dissociation constants from Marion and Kargel (2008) showed that neglecting $m_{CO_3^{2-}}$, m_{H^+} and m_{OH^-} would result in an error of < 1.7% within the studied temperature range.
2) Systematic errors in the m_{TA} measurement associated with the liquid junction potential when titrating the concentrated solutions with the HCl titrant that was not matrix-matched. To provide a conservative estimate of this error, the liquid junction potentials of the glass electrode in each solution were calculated according to Marino et al. (2014). The appropriate junction potentials were applied to the experimentally determined Gran Plot of the trial with the largest dilution, allowing a re-calculation of TA. The difference between the recalculated and measured TA was treated as a maximum error due to changes in salinity over the course of a titration. The results showed a maximum underestimate of 1.6 μmol kg^{-1}, which is < 1.5% of the desired accuracy to allow ($m_{DIC} - m_{TA}$) > 10^{-4} mol kg^{-1}.
3) Random errors associated with the measurements of m_{DIC}, m_{TA} and pCO_2 in each experimental run. These can be estimated in a multi-step process. First, the random errors associated with replicate measurements of m_{DIC} and m_{TA} were calculated using student's t values for a 95% confidence limit, taking into consideration errors involved in the measurements of volume, mass, and density. Measurement variations in pCO_2 from the continually measured output of the LI-COR-7000 NIR detector were found to be smaller than 1% in all trials; thus, a 1% relative error was used in calculations as a conservative estimate. These errors were then propagated to determine the uncertainty, as standard deviation, associated with K_H^* and K_H.

$$s_{K_H^*} = K_H^* \sqrt{\left(\frac{\sqrt{s_{DIC}^2 + s_{TA}^2}}{m_{DIC} - m_{TA}}\right)^2 + \left(\frac{s_{pCO_2}}{pCO_2}\right)^2} \quad (13)$$

$$s_{K_H} = \frac{\gamma_{CO_2(g)}}{\gamma_{CO_2(aq)}} \; s_{K_H^*} \quad (14)$$

4) Random errors associated with the replicate runs under the same T-S conditions. These can be estimated by the standard deviation of the means from the replicate runs. Trials at each temperature and salinity were run until a minimum of three results agreed within or below a relative standard deviation of 10%. A two-sided Grubbs outlier test was conducted on each result, and found no significant outliers at p = .05.

The overall uncertainties associated with K_H, as shown in Table 2, were dominated by the fourth source. In general, higher uncertainties were observed with the values obtained at the two lowest temperatures, −5 and −10 °C, but the overall standard deviations were always < 0.1 logarithm units.

It should be noted that the above estimate of uncertainties did not include the uncertainties associated with the calculation of the activity coefficients γ_{CO_2}(g) and γ_{CO_2}(aq) for the determination of K_H (Eq. (14)). Although the Pitzer approach (Pitzer, 1995) is the most commonly used method for estimating activity coefficients in highly concentrated solutions, the uncertainties associated with this empirical approach remain unquantified. Nevertheless, the observation that experiments carried out at the same temperature at very different ionic strengths resulted in different K_H^* values but the K_H values converged (e.g., at −1 and − 2 °C) suggests that the use of the Pitzer approach was appropriate.

5. Discussion

5.1. Validity of the new approach in determining K_H

The major advantage of the pCO_2-DIC-TA approach used in this study is that, as long as the experimental conditions are controlled so that Eq. (9) is valid, the determination of K_H does not involve any other thermodynamic constants for the CO_2-carbonate system at sub-zero temperatures, nor does it rely on the accurate measurement of pH under such conditions. The validity of this approach is compared with K_H values determined previously in other experimental studies.

Prior to the study at sub-zero temperatures, a test run was carried out to determine K_H for CO_2 at the room temperature (21.8 °C, in 34.9 g NaCl (kg solution)$^{-1}$). The K_H was determined to be 3.41×10^{-2} mol (kg H_2O)$^{-1}$, which agrees, within 8% of the relative error, with the K_H value of 3.19×10^{-2} mol (kg H_2O)$^{-1}$ reported at 22 °C in artificial

Table 1
Experimental results for the determination of the stoichiometric (K_H^*) and thermodynamic (K_H) Henry's Law constants for CO_2 under low temperature and high salinity conditions.

t	T	Salinity	pH[a]	pCO_2	TA	DIC	K_H^*	$\gamma_{CO_2}(aq)$[b]	$\gamma_{CO_2}(g)$[b]	K_H
°C	K	g NaCl (kg solution)$^{-1}$		μatm	μmol (kg H_2O)$^{-1}$	μmol (kg H_2O)$^{-1}$	mol (kg H_2O)$^{-1}$ atm^{-1}			mol (kg H_2O)$^{-1}$ atm^{-1}
−1.0	272.15	34.9	7.05	1918	760.1	904.3	7.52×10^{-2}	1.167	0.993	8.84×10^{-2}
−1.0	272.15	34.9	7.15	1642	823.0	959.9	8.34×10^{-2}	1.167	0.993	9.80×10^{-2}
−1.0	272.15	34.9	7.06	1983	807.4	952.9	7.34×10^{-2}	1.167	0.993	8.63×10^{-2}
−1.0	272.15	34.9	7.13	1707	808.3	941.4	7.80×10^{-2}	1.167	0.993	9.17×10^{-2}
−1.0	272.15	108.8	6.99	1786	740.2	839.1	5.54×10^{-2}	1.654	0.993	9.23×10^{-2}
−1.0	272.15	108.8	6.94	2016	740.6	837.8	4.82×10^{-2}	1.654	0.993	8.04×10^{-2}
−1.0	272.15	108.8	6.94	1925	720.1	822.6	5.33×10^{-2}	1.654	0.993	8.87×10^{-2}
−1.0	272.15	151.9	6.87	2488	829.3	928.8	4.00×10^{-2}	2.111	0.993	8.50×10^{-2}
−1.0	272.15	151.9	6.91	2339	846.1	943.1	4.15×10^{-2}	2.111	0.993	8.81×10^{-2}
−1.0	272.15	151.9	6.97	2001	825.3	908.4	4.15×10^{-2}	2.111	0.993	8.82×10^{-2}
−2.0	271.15	108.8	6.97	1876	757.5	869.2	5.95×10^{-2}	1.666	0.993	9.99×10^{-2}
−2.0	271.15	108.8	7.02	1656	752.1	854.3	6.17×10^{-2}	1.666	0.993	1.04×10^{-1}
−2.0	271.15	108.8	6.96	1736	687.1	797.1	6.34×10^{-2}	1.666	0.993	1.06×10^{-1}
−2.0	271.15	151.9	6.87	1867	629.4	709.0	4.27×10^{-2}	2.130	0.993	9.16×10^{-2}
−2.0	271.15	151.9	6.91	1732	630.8	718.1	5.04×10^{-2}	2.130	0.993	1.08×10^{-1}
−2.0	271.15	151.9	6.88	1806	621.5	700.5	4.37×10^{-2}	2.130	0.993	9.38×10^{-2}
−5.0	268.15	151.9	6.95	1459	620.2	678.7	4.01×10^{-2}	2.201	0.993	8.89×10^{-2}
−5.0	268.15	151.9	7.00	1309	623.7	685.7	4.73×10^{-2}	2.201	0.993	1.05×10^{-1}
−5.0	268.15	151.9	6.94	1467	612.4	706.6	6.43×10^{-2}	2.201	0.993	1.42×10^{-1}
−10.0	263.15	151.9	7.22	1802	860.1	988.2	7.11×10^{-2}	2.380	0.992	1.71×10^{-1}
−10.0	263.15	151.9	6.97	1911	857.4	946.8	4.68×10^{-2}	2.380	0.992	1.12×10^{-1}
−10.0	263.15	151.9	6.90	2008	772.6	902.1	6.45×10^{-2}	2.380	0.992	1.55×10^{-1}
−10.0	263.15	151.9	6.93	1722	708.0	806.1	5.70×10^{-2}	2.380	0.992	1.37×10^{-1}
−10.0	263.15	151.9	6.86	2094	726.3	849.9	5.90×10^{-2}	2.380	0.992	1.42×10^{-1}
21.8[c]	294.95	34.9	6.61	3075	3925	4017	3.0×10^{-2}	1.132	0.995	3.41×10^{-2}

[a] Estimated from FREZCHEM.
[b] Activity coefficients were calculated from FREZCHEM.
[c] This was a test run for comparison with previous work at above-zero temperatures.

Table 2
Thermodynamic Henry's Law constants (K_H) for CO_2 under low temperature and high salinity conditions.

t	T	K_H [mol (kg H_2O)$^{-1}$ atm^{-1}]		Difference (%)
°C	K	Plummer and Busenberg (1982)	This study	
−1.0	272.15	8.11×10^{-2}	$(8.87 \pm 0.47) \times 10^{-2}$	−8.6
−2.0	271.15	8.45×10^{-2}	$(1.01 \pm 0.07) \times 10^{-1}$	−16.3
−5.0	268.15	9.60×10^{-2}	$(1.12 \pm 0.28) \times 10^{-1}$	−14.3
−10.0	263.15	1.20×10^{-1}	$(1.43 \pm 0.22) \times 10^{-1}$	−16.1

seawater, as calculated by Weiss (1974) from the experimental data of Murray and Riley (1971).

The only other experimentally determined CO_2 solubility at sub-zero temperatures was given by Stewart and Munjal (1970). At −5 °C in synthetic seawater (S = 34), the solubility of CO_2 was determined to be 3.1 g CO_2 (kg seawater)$^{-1}$ at pCO_2 = 1 atm, which is equivalent to a K_H of 1.07×10^{-1} mol (kg H_2O)$^{-1}$ atm^{-1}. This value agrees, within 5% of the relative error, with the K_H value we obtained at the same temperature (1.12×10^{-1} (kg H_2O)$^{-1}$ atm^{-1}), despite the fact that our value was determined at a much higher salinity (151.9) in NaCl solution.

The good agreement in K_H at both 21.8 and − 5 °C with previously reported values suggests that the pCO_2-DIC-TA approach used in this study is valid and that the conditions required by Eq. (9) were met during the experiments. The agreement of the K_H values determined in different media (NaCl solution versus artificial seawater) and salinities also confirms that the K_H determined is matrix independent and can be applied to different media.

5.2. Comparison with extrapolated results

Various extrapolation equations are available in the literature to estimate the solubility of CO_2 at sub-zero temperatures, all of which were based on experimental data that were determined at above 0 °C. For instance, geochemical models such as FREZCHEM (Marion and Kargel, 2008) use a $K_H - T$ function derived by Plummer and Busenberg (1982):

$$\ln K_H = 2.495691 \times 10^2 + 4.570806 \times 10^{-2}T - 1.593281 \times 10^4/T - 4.045154 \times 10 \ln(T) + (1.541270 \times 10^6)T^2 \quad (273 \leq T \leq -598 \text{ K}) \tag{15}$$

As shown in Table 2 and Fig. 2a,b, whereas this empirical function predicts the increasing trend in K_H as T decreases into the sub-zero regime, it underestimates the sub-zero temperature K_H values by 9% to 16%, with greater discrepancy at lower temperatures. Attempts to update Eq. (15) to include our new data for sub-zero temperatures were not successful due to a slope change at ~0 °C. Instead, a new fitting equation was derived for the sub-zero temperatures only (R^2 = 0.991, n = 5):

$$\ln K_H = -2.484 + 2.775 \times 10^{-2}(274 - T) - 9.854 \times 10^{-2}/(274 - T) - 1.009 \times 10^{-1} \ln(274 - T) \quad (263 \leq T < 273 \text{ K}) \tag{16}$$

The fit of the experimental data to Eq. (16) for sub-zero temperatures is shown in Fig. 2c. A comparison between Fig. 2b and c shows that the $K_H - T$ function derived by Plummer and Busenberg (1982) should not be extended to sub-zero temperatures, for which the new $K_H - T$ function of Eq. (16) should be used instead.

It remains unclear why there is a slope change in K_H around 0 °C. There could be due to inconsistencies in our values and literature values because of different methods used. However, the good agreement in K_H

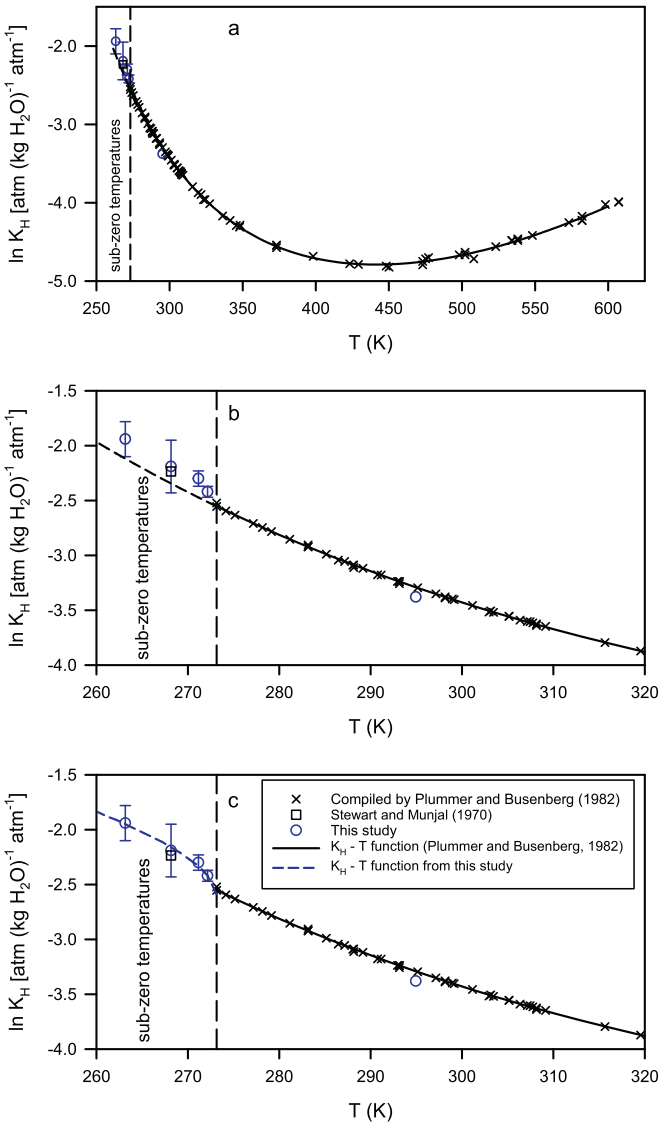

Fig. 2. Comparison of the thermodynamic K_H values obtained for sub-zero temperatures with those reported for above-zero temperatures (Plummer and Busenberg, 1982). A) The full temperature range from 260 to 600 K; B) A zoomed-in version to show the temperature range (260 to 320 K) that is relevant to the surface oceans. Error bars show the standard deviation. C) Same as B), but with a new K_H-T function shown for the sub-zero temperatures.

at both a sub-zero (−5 °C) and above-zero (21.8 °C) temperature between our and literature values, as discussed earlier, suggests that methodological differences are unlikely the reason. Further studies are warranted to determine K_H within a narrow temperature range around 0 °C to resolve the cause of its discontinuity between sub-zero and above-zero temperatures.

5.3. Implication for the climate modeling

While geochemical models use the salinity-independent thermodynamic K_H, climate-carbon cycle models tend to use the stoichiometric Henry's Law constant that is dependent on salinity. Most coupled climate-carbon cycle models (Orr et al., 2017) parameterize the solubility of CO_2 in seawater from the $K_0 - T - S$ function derived by Weiss (1974):

$$\ln\ K_0[\text{mol (kg sw)}^{-1}\text{atm}^{-1}] = -60.2409 + 93.4517\frac{100}{T} + 23.3585\ \ln\frac{T}{100} + S\left[0.023517 - 0.023656\frac{T}{100} + 0.0047036\left(\frac{T}{100}\right)^2\right] \quad (17)$$

Note that K_0 in Eq. (17) is expressed in gravimetric units. Eq. (17) was derived from a reanalsis of experimental data of Murray and Riley (1971) under above-zero temperature conditions ($1 \le t \le 35$°C; $0 \le S \le 37.4$).

In polar regions, air-sea exchange of CO_2 occurs generally in open water and within openings in sea ice including polynyas, cracks and leads. Air-sea exchange of CO_2 for ice-covered regions is typically estimated using generic models (e.g., Wanninkhof (2014)) applied to the open water fraction in conjunction with open water properties, in which the CO_2 solubility is also estimated by Eq. (17). With the K_H values determined from this work, K_0 under sub-zero temperature conditions ($-10 \le t \le -1$ °C; $35 \le S \le 152$) can be calculated from:

$$K_0[\text{mol (kg sw)}^{-1}\text{atm}^{-1}] = \frac{[CO_2(aq)]\ [\text{mol (kg sw)}^{-1}]}{p_{CO_2}\ [\text{atm}]} = (1 - 0.001S)\frac{\gamma_{CO_2(g)}}{\gamma_{CO_2(aq)}}K_H\ [\text{mol (kg H}_2\text{O)}^{-1}\ \text{atm}^{-1}] \quad (18)$$

As shown in Table 3, when applied to sub-zero temperatures, the Weiss equation (Eq. 17) can underestimate the K_0 values by up to 19%.

Sensitivity analyses are thus needed for modeling studies to determine how such an underestimate of the CO_2 solubility in sub-zero seawater would affect air-sea exchange of CO_2 in polar oceans and the ocean carbonate system, as well as regional and global climate projections under various CO_2 emission scenarios.

6. Conclusion

This study determined, for the first time, the Henry's Law constant K_H for CO_2 in NaCl solutions to sub-zero temperatures (−1 to −10 °C) and salinities (34.9 to 151.9 in NaCl) that resemble the conditions of freezing seawater and sea-ice brine in polar oceans. As the K_H is expressed in thermodynamic terms (i.e., activity of solutes and fugacity of the gas, corrected for ionic strength), the values and equation derived from our measurements are independent of the chemical composition of the fluid and should be applicable to the polar marine and sea-ice environment. The results show that the general practice, in geochemical and coupled climate-carbon cycling models, of extrapolating K_H values from above-zero to sub-zero temperatures underestimates the solubility of CO_2 by 9%–19% between the temperatures of −1 and −10 °C. Together with the recent determinations of sub-zero temperature dissociation constants of carbonic acids (Papadimitriou et al., 2018) and

Table 3
Stoichiometric Henry's Law constants (K_0) for CO_2 under low temperature and high salinity conditions.

t	T	Salinity	K_0 [mol (kg sw)$^{-1}$ atm^{-1}]		
°C	K		Weiss (1974)	This study[a]	Difference (%)
−1.0	272.15	34.9	6.54×10^{-2}	7.28×10^{-2}	−10.2
		108.8	4.19×10^{-2}	4.75×10^{-2}	−11.2
		151.9	3.23×10^{-2}	3.54×10^{-2}	−8.6
−2.0	271.15	108.8	4.36×10^{-2}	5.37×10^{-2}	−18.8
		151.9	3.36×10^{-2}	3.99×10^{-2}	−15.9
−5.0	268.15	151.9	3.78×10^{-2}	4.29×10^{-2}	−11.8
−10.0	263.15	151.9	4.67×10^{-2}	5.05×10^{-2}	−7.6

[a] Calculated from Eq. (18).

solubility product of ikaite (Papadimitriou et al., 2013), the sub-zero temperature carbonate chemistry needs to be better represented in geochemical and climate models to fully understand the role of the polar oceans in global CO_2 cycling and the coupled feedback with climate change.

Acknowledgements

This work was supported by the Natural Sciences and Engineering Research Council (NSERC) of Canada (F.W. and T.P.), the Canada Research Chairs Program (F.W.), and the ArcticNet Networks of Centres of Excellence (F.W. and T.P.). We thank Debbie Armstrong, Yubin Hu, and Nicolas-Xavier Geilfus for their assistance in the laboratory. We are grateful to Associate Editor Dr. Alfonso Mucci and two anonymous reviewers for their thorough and insightful comments on an earlier version, which have significantly improved the quality of this paper.

References

Anderson, L.G., Falck, E., Jones, E.P., Jutterstrom, S., Swift, J.H., 2004. Enhanced uptake of atmospheric CO_2 during freezing of seawater: a field study in Storfjorden, Svalbard. J. Geophys. Res. Oceans 109, C06004. https://doi.org/10.1029/2003JC002120.

Carroll, J.J., Slupsky, J.D., Mather, A.E., 1991. The solubility of carbon dioxide in water at low presssure. J. Phys. Chem. Ref. Data 20, 1201–1209.

Dickson, A.G., Afghan, J.D., Anderson, G.C., 2003. Reference materials for oceanic CO2 analysis: a method for the certification of total alkalinity. Mar. Chem. 80, 185–197.

Dieckmann, G.S., et al., 2008. Calcium carbonate as ikaite crystals in Antarctic sea ice. Geophys. Res. Lett. 35, L08501,. https://doi.org/10.1029/2008GL033540.

Dieckmann, G.S., et al., 2010. Ikaite ($CaCO_3{\cdot}6H_2O$) discovered in Arctic sea ice. Cryosphere 4, 227–230.

Grimm, R., Notz, D., Glud, R.N., Rysgaard, S., Six, K.D., 2016. Assessment of the sea-ice carbon pump: Insights from a three-dimensional ocean-sea-ice-biogeochemical model (MPIOM/HAMOCC). Elementa 4, 000136,. https://doi.org/10.12952/journal.elementa.000136.

Hare, A.A., et al., 2013. pH evolution in sea ice grown at an outdoor experimental facility. Mar. Chem. 154, 46–54.

He, S., Morse, J.W., 1993. The carbonic acid system and calcite solubility in aqueous Na-K-Ca-Mg-Cl-SO_4 solutions from 0 to 90 °C. Geochim. Cosmochim. Acta 57, 3533–3554.

Khatiwala, S., et al., 2013. Global ocean storage of anthropogenic carbon. Biogeosciences 10, 2169–2191.

Le Quéré, C., et al., 2016. Global carbon budget 2016. Earth Syst. Sci. Data 8, 605–649.

Marino, M., Misuri, L., Brogioli, D., 2014. A New Open Source Software for the Calculation of the Liquid Junction Potential Between Two Solutions According to the Stationary Nernst-Planck Equation. (eprint arXiv:1403.3640v2).

Marion, G.M., Kargel, J.S., 2008. Cold Aqueous Planetary Geochemistry With FREZCHEM: From Modeling to the Search for Life at the Limits. Springer, Heideberg (251 pp).

Meier, W.N., 2017. Losing Arctic sea ice: observations of the recent decline and the long-term context. In: Thomas, D.N. (Ed.), Sea Ice, 3rd ed. Wiley-Blackwell, London, pp. 290–303.

Miller, L.A., et al., 2011. Carbon dynamics in sea ice: a winter flux time series. J. Geophys. Res. Oceans 116, C02028,. https://doi.org/10.1029/2009jc006058.

Millero, F.J., 2013. Chemical Oceanography, 4th ed. CRC Press, Boca Raton, FL, USA.

Moreau, S., et al., 2016. Assessment of the sea-ice carbon pump: Insights from a three-dimensional ocean-sea-ice-biogeochemical model (NEMO-LIM-PISCES). Elementa 4, 000122,. https://doi.org/10.12952/journal.elementa.000122.

Murray, C.N., Riley, J.P., 1971. The solubility of gases in distilled water and sea water – IV. Carbon dioxide. Deep-Sea Res. 18, 533–541.

Orr, J.C., et al., 2017. Biogeochemical protocols and diagnostics for the CMIP6 Ocean Model Intercomparison Project (OMIP). Geosci. Model Dev. 10, 2169–2199.

Papadimitriou, S., Kennedy, H., Kennedy, P., Thomas, D.N., 2013. Ikaite solubility in seawater-derived brines at 1 atm and sub-zero temperatures to 265 K. Geochim. Cosmochim. Acta 109, 241–253.

Papadimitriou, S., et al., 2018. The stoichiometric dissociation constants of carbonic acid in seawater brines from 298 to 267 K. Geochim. Cosmochim. Acta 220, 55–70.

Pitzer, K.S., 1995. Thermodynamics, 3rd ed. McGraw-Hill, New York (626 pp).

Plummer, L.N., Busenberg, E., 1982. The solubilities of calcite, aragonite and valerite in CO_2-H_2O solutions between 0 and 90°C, and an evaluation of the aqueous model for the system $CaCO_3$-CO_2-H_2O. Geochim. Cosmochim. Acta 46, 1011–1040.

Potter, R.W., Clynne, M.A., Brown, D.L., 1978. Freezing point depression of aqueous sodium chloride solutions. Econ. Geol. 73, 284–285.

Rysgaard, S., Glud, R.N., Sejr, M.K., Bendtsen, J., Christensen, P.B., 2007. Inorganic carbon transport during sea ice growth and decay: a carbon pump in polar seas. J. Geophys. Res. 112 (C3). https://doi.org/10.1029/2006JC003572.

Rysgaard, S., et al., 2011. Sea ice contribution to the air-sea CO_2 exchange in the Arctic and Southern Oceans. Tellus B 63, 823–830.

Rysgaard, S., et al., 2013. Ikaite crystal distribution in winter sea ice and implications for CO_2 system dynamics. Cryosphere 7, 707–718.

Rysgaard, S., et al., 2014. Temporal dynamics of ikaite in experimental sea ice. Cryosphere 8, 1469–1478.

Sarmiento, J.L., Gruber, N., 2006. Ocean Biogeochemical Dynamics. Princeton University Press, Princeton, NJ (503 pp).

Stewart, P.B., Munjal, P.K., 1970. Solubility of carbon dioxide in pure water, synthetic sea water, and synthetic sea water concentrates at –5° to 25 °C and 10- to 45 atm. pressure. J. Chem. Eng. Data 15, 67–71.

Takahashi, T., et al., 2009. Climatological mean and decadal change in surface ocean pCO_2, and net sea–air CO_2 flux over the global oceans. Deep Sea Res. II 56, 554–577.

Takahashi, T., et al., 2014. Climatological distributions of pH, pCO_2, total CO_2, alkalinity, and $CaCO_3$ saturation in the global surface ocean, and temporal changes at selected locations. Mar. Chem. 164, 95–125.

Wanninkhof, R., 2014. Relationship between wind speed and gas exchange over the ocean revisited. Limnol. Oceanogr. Methods 12, 351–362.

Weiss, R.F., 1974. Carbon dioxide in water and sea water. Solubility of a nonideal gas. Mar. Chem. 2, 203–215.